ADVANCED MATERIALS INTERFACES
Open Access
www.advmatinterfaces.de

Synthetic Plant Cuticle Coating as a Biomimetic Moisture Barrier Membrane for Structurally Colored Cellulose Films

Prasaanth Ravi Anusuyadevi, Shuvra Singha, Debashree Banerjee, Magnus P Jonsson, Mikael S. Hedenqvist, and Anna J. Svagan**

Photonic films based on cellulose nanocrystals (CNCs) are sustainable candidates for sensors, structurally colored radiative cooling, and iridescent coatings. Such CNC-based films possess a helicoidal nanoarchitecture, which gives selective reflection with the polarization of the incident light. However, due to the hygroscopic nature of CNCs, the structural colored material changes and may be irreversibly damaged at high relative humidity. Thus, moisture protection is essential in such settings. In this work, hygroscopic CNC-based films are protected with a bioinspired synthetic plant cuticle; a strategy already adopted by real plants. The protective cuticle layers altered the reflected colors to some extent, but more importantly, they significantly reduced the water vapor permeance by more than two orders of magnitude, from 2.1×10^7 (pristine CNC/GLU film) to 12.3×10^4 g µm m^{-2} day^{-1} atm^{-1} (protected CNC/GLU film). This expands significantly the time window of operation for CNC/GLU films at high relative humidity.

1. Introduction

The protective outer cuticle membrane, present on all aboveground organs of plants such as leaves and fruits, is a vital transpiration barrier that regulates water loss between plants and the atmosphere – without it these would suffer from lethal wilting and/or shrinking.[1] The water barrier properties of this extracellular membrane surpass most common synthetic polymer films, such as polyethylene (PE), polypropylene, and poly(ethylene terephthalate).[2] The cuticle system is a layered structure that comprises, amongst others, an upper epicuticular wax layer and a layer containing cutin polyester and wax blended with cell wall polysaccharides, such as cellulose and pectin, see **Figure 1**.[3] The hydrophobic cutin polyester structure, closely resembles that of PE, due to the long alkane chain monomeric units (10,16-dihydroxyhexadecanoic acid and 16-hydroxyhexadecanoic acid in the C_{16} family, and 18-hydroxy-9,10-epoxyoctadecanoic acid and 9,10,18-trihydroxyoccadecanoic acid in the C_{18} family are predominant).[4] The barrier properties of cutin polymer membranes depend on the polyester chain packing, crystallinity, and cross-link density (with glycerol: natural crosslinker in plants). Many efforts have been devoted to produce synthetic cutin membranes with controlled crystallinity and cross-link density to tailor physical properties, most importantly, achieving adequate barrier and mechanical properties to design sustainable materials.[5]

Cellulose nanocrystals (CNCs) are unique due to their intrinsic ability to self-assemble into nanophotonic structures with distinct structural colors.[6] This characteristic property of structural colors has found its use in several fields including sensors (polarization sensor[7] colorimetric sensor for the detection of gases[8] and humidity sensor[9,10]), optical anti-counterfeiting systems[11] decorative coatings[12] colored radiative cooling[13] and rewritable papers.[14] The structural colors in CNC-based films are a consequence of constructive interference (Bragg's law) of reflected light, and by controlling the cholesteric pitch (the distance of a full-turn period), certain wavelengths will be reflected only.[15,16] The height of the pitch can be fine-tuned by intercalating molecules, such as glucose,[16] poly(ethylene glycol)[10] polyacrylamide,[9] hydroxypropyl cellulose,[17] glycerol,[18] polyethylene glycol diacrylate,[19] and this will result in different reflected colors. In the present study, glucose was used to modulate the pitch. The helical CNC arrangement and pitch are, however, sensitive to water up-take, which swells the material and increases the pitch.[10] This is due to the hygroscopic properties of glucose and CNC-based materials. Moreover, we selected glucose as a model molecule due to its moisture sensitivity, that is, exposure to moisture might induce

P. R. Anusuyadevi, S. Singha, M. S. Hedenqvist, A. J. Svagan
Royal Institute of Technology (KTH)
Dept. of Fibre and Polymer Technology
Stockholm SE-100 44, Sweden
E-mail: ranu.prasaanth@gmail.com; svagan@kth.se

P. R. Anusuyadevi
M S Ramaiah Institute of Technology
Dept. of Chemical Engineering
Bangalore, Karnataka 560054, India

D. Banerjee, M. P. Jonsson
Linköping University
Laboratory of Organic Electronics and Wallenberg Wood Science Center
Dept. of Science and Technology
Norrköping SE-601 74, Sweden

The ORCID identification number(s) for the author(s) of this article can be found under https://doi.org/10.1002/admi.202202112.

DOI: 10.1002/admi.202202112

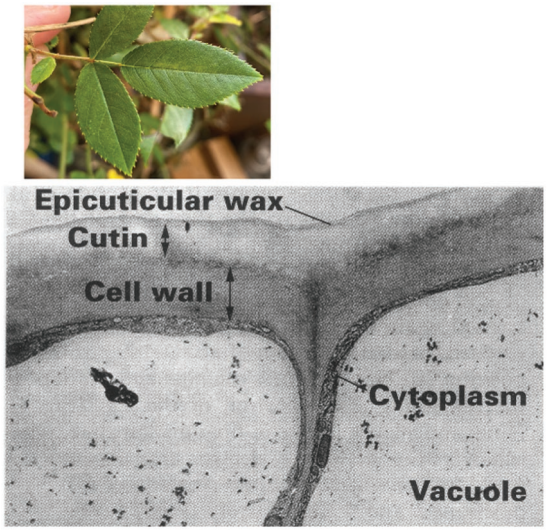

Figure 1. The plant cuticles form the outer barrier on leaves. The layered structure (TEM, transverse section) of the plant cuticle of a leaf (Clivia miniata). The cutin layer contains polysaccharides. The TEM micrograph is reproduced with permission.[3] Copyright 2000, John Wiley & Sons.

the growth of glucose crystals in CNC/GLU films. Hence, there is a need to protect these materials from water in order to avoid variable structural colors when in operation in ambient conditions. Indeed, the relative humidity will vary between night and day, and also seasons.[20]

In the present study, we take a cue from nature and protect structurally colored CNC/glucose films from moisture by introducing a synthetic cuticle coating on top of the films' surfaces. The films' morphology and structural colors were investigated with optical microscopy, scanning electron microscopy, and UV–vis spectroscopy, and the moisture barrier properties were measured with the cup test and compared with those obtained for the uncoated films.

2. Experimental Section

2.1. Materials

D-(+)-Glucose (GLU) (purity ≥ 99.5%), 16-Hydroxyhexadecanoic acid (HHA) (98%), and glycerol (>99%) were obtained from Sigma–Aldrich. Microcrystalline cellulose MCC Avicel PH-200 was bought from DuPont and sulfuric acid (95–97%) was supplied by Merck. All chemicals were used as received.

2.2. Preparation of CNCs

Cellulose Nanocrystals were prepared using the protocol reported in our previous work[16] with some slight modifications. 20 g of MCC was hydrolyzed for 75 min at 45 °C with intense magnetic stirring using sulfuric acid (247 g of 64 wt.%). Subsequently, the reaction was quenched by diluting the reaction medium with tenfold Milli-Q water and the resultant suspension was unperturbed overnight. The next day, the supernatant (≈1 L) was discarded and the remaining sediment was ultrasonicated with a 90% amplitude for 2 min (1/2-inch tip, Vibra-Cell VCX 750, Sonics & Materials), followed by centrifugation at 15 000 rpm (rcf = 26 964 g, SORVALL RC 5B PLUS centrifuge, Fiberlite F21-8 × 50y rotor) for 5 min. The supernatant was discarded and the remaining sediment in the centrifuge tubes was redispersed in Milli-Q water. This centrifugation procedure was repeated thrice, after which only the supernatant was collected and dialyzed using a cellulose membrane tube (14 kDa molecular weight cut-off) for 10 days. Then, the dialyzed suspension was filtered using a Whatman Grade 541 filter paper. The CNC suspension was concentrated to 3.2 wt.% with a surface charge of 0.37 mmol g^{-1}, measured using the procedure employed previously.[16]

2.3. Synthesis of Hydroxyhexadecanoic Acid – Glycerol Copolymer

The polyester was synthesized as described previously by Singha et al.[4] Briefly, 150 mg of 16-hydroxyhexadecanoic acid monomer was reacted with glycerol (Gly) at the molar ratio of HHA: Gly = 3:1. The HHA was melted in a round-bottom flask (at 110 °C) and glycerol was added to the melt, see schematic in **Scheme 1**. The mixture was stirred vigorously for 24 h at 110 °C. The mixture was cooled and the solidified HHA-glycerol mixture was then ground to powder. The powdered mixture was heated at 150 °C in an oven for 24 h followed by cooling to room temperature. A second thermal treatment at 160 °C (24 h) was then performed and the crosslinked polymer, thus

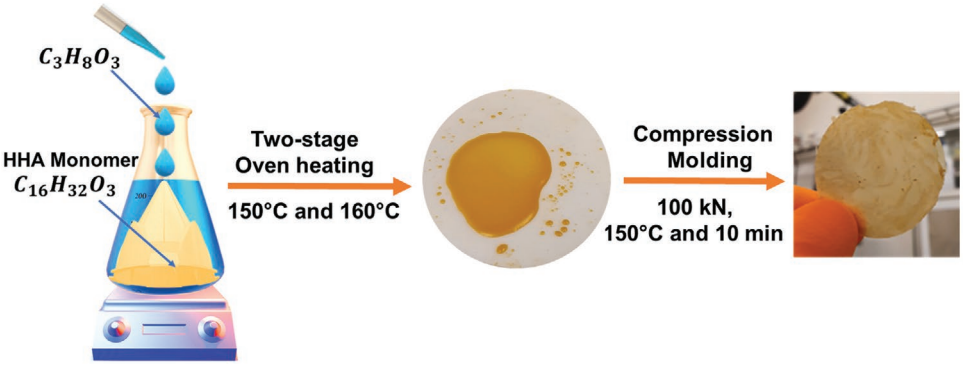

Scheme 1. Schematic representation of the subsequent synthetic protocols for realizing thick HG31 (HHA: Glycerol = 3:1) polyester films.

obtained, was cut into pieces and stored for further processing. In the previous article it was referred to as HHA: Gly = 3:1, here we will use a shorter name HG31.

2.4. CNC/Glucose Film Preparation

2.4.1. Fabrication of the CNC/GLU (52/48) film

To 4.8 ml of 3.2 wt.% CNC suspension, 140 mg of glucose, and 15.2 ml of Milli-Q water was added in a closed glass vial. The mixture was magnetically stirred for 16 h at room temperature. Then, the suspension was solvent-casted in a polystyrene petri dish (diameter: 6 cm) and dried in ambient lab conditions for 3, 4 days.

2.4.2. Fabrication of CNC/GLU (39/61) film

To 1.6 ml of 3.2 wt.% CNC suspension, 80 mg of glucose, and 8.4 mL Milli-Q water were added. The suspension, present in closed glass vials, was stirred magnetically for 16 h. Subsequently, the suspension was solvent-casted in a polystyrene petri dish and dried in ambient lab conditions for 2, 3 days.

2.4.3. Fabrication of Pristine CNC film

10 ml of 3.2 wt.% CNC suspension was solvent casted and dried in ambient lab conditions for 2, 3 days.

2.5. Preparation of HG31-Laminated CNC/GLU Films and Thin HG31 Films

The HG31 polymer was cut into small pieces and uniformly spread in circular molds of 3 cm diameter and 150 µm thickness and sandwiched between steel plates with poly(tetrafluoro ethylene) (PTFE) anti-sticking sheets in between the material and the plate. The material was first heated to 150 °C for 10 min to melt the polymer, followed by hot-pressing (Fontijne Press, TP 400) at the same temperature (150 °C) for another 10 min at 100 kN force. The obtained thick HG31 film is shown in Scheme 1.

2.5.1. Thin HG31 film fabrication

A thick HG31 film (150 µm) was subjected to 160 °C, 250 kN for 10 min using the same hot-press, compression plates, and PTFE sheets as described above, but without a mold. A temperature of 160 °C was selected during hot-pressing because recent studies on similar polyester films showed that temperatures beyond 175 °C might cause degradation of the polymer through oxidation of the moieties on the surface.[32]

2.5.2. Fabrication of artificial cuticle laminated CNC/GLU film

Two of the thin (≈40 µm) HG31 films were used to cover each side of a CNC/GLU film (either a CNC/GLU = 52/48 or a CNC/GLU = 39/61 film), and the sandwich structure was compressed further (25 °C, 250 kN for 10 min with the same hot-press, compression plates and PTFE sheets assembly as described above) to create the synthetic cuticle coating.

2.6. Characterization

Scanning electron microscopy images were obtained at an accelerating voltage of either 3, 5, or 10 kV using a Hitachi S-4800 SEM equipment. Specifically, 5 kV was used for **Figure 2**f and 10 kV for Figure 4e. Cross-sectionally dissected samples were prepared by first freezing pristine pieces of CNC/Glucose film, synthetic cuticle film, and the HG31-laminated CNC/Glucose films in liquid nitrogen for 5 min. Each frozen sample was then cut using a lancet. These cross-sectionally anatomized films were mounted on Al-stubs and subsequently sputter-coated with Pt/Pd (60/40) for a duration of 10 s resulting in a coating thickness of ≈1 nm, using a Cressington 208HR sputter coater equipment.

Polarized optical reflection measurements were performed at normal incidence using linearly polarized incident light only and a custom-made polarization-dependent micro-spectroscopic setup. The reflected light was collected from the camera port with an optical fiber (Thorlabs; 150 µm) core connected to a spectrometer (Ocean OpticsHR 4000, USA). Imaging was performed either using linearly polarized incident light or with two crossed linear polarizers. Samples were illuminated using a 50 W halogen lamp attached to a microscope (Nikon Eclipse L200N, Japan).

Polarized optical microscopy images in transmission mode between crossed polarizers (linearly polarized light) were obtained using a Leitz Ortholux II light microscope equipped with a 6.3× POL objective and a Leica DMC2900 Digital Microscope camera. The sample was rotated counter-clockwise from 0 to 135° using 45° steps.

Polarized optical microscopy images between crossed polarizers in reflection (linearly polarized light, images in Figure 2d,e,i) were obtained using a Leica DM750M (Leica, Germany) microscope equipped with 5×, 10× and 20× POL objectives and a Leica ICC50W camera.

UV–vis spectrometry measurements to obtain direct transmittance, total transmittance (measuring both linear and scattered components through the sample) and diffuse reflectance (illumination at 0°, angle of incident), and total reflectance (illumination at 8°, angle of incident) measurements were performed using a UV–vis spectrophotometer (Shimadzu UV 2550). In the case of total transmittance and reflectance measurements, an integrating sphere setup (model ISR-2200) was used. $BaSO_4$ was used as the standard reference in the integrating sphere setup and to perform the baseline correction. To calculate the absorptance ($A(\lambda)$), the total reflectance ($R(\lambda)$) and the total transmittance ($T(\lambda)$) was used:

$$A(\lambda) = 1 - T(\lambda) - R(\lambda) \quad (1)$$

To assess the influence of humidity on the direct transmittance spectrum (Figure 2g), measurements were performed on a CNC/GLU (52/48) film mounted on a microscopy slide. The

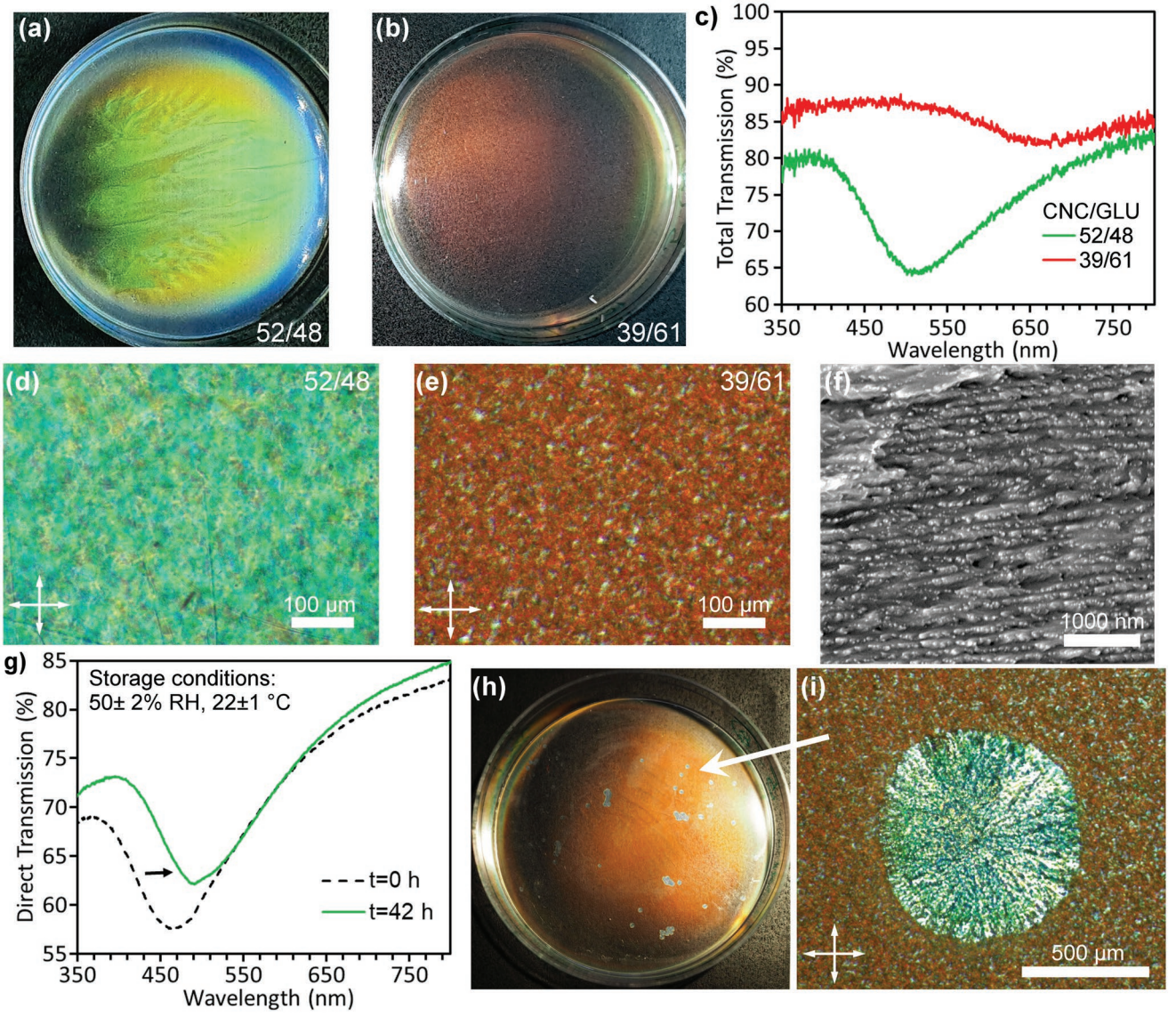

Figure 2. In a,b) photographs of CNC/GLU films with different compositions. c) Total transmittance spectra of the films in (a) and (b). Films were equilibrated at 50 ± 2% RH, 22 ± 1 °C. In d,e) POM images (crossed linear polarizers, reflection mode) of CNC/GLU films. In f) SEM image of a cross-section of a CNC/GLU film (52/48). In g) red-shifting of UV–vis spectrum due to moisture-induced swelling (increased pitch). At t = 0 h the film was dry. h) Long time exposure of a CNC/GLU film (39/61 (>6 months, ambient room conditions). i) POM image of one formed glucose crystal in the CNC/GLU film in (h).

film was first dried in a desiccator with silica gel for 2 weeks and directly measured (t = 0), then the specimen was placed at 50 ± 2% RH and 22 ± 1 °C for 42 h and remeasured.

2.6.1. Water vapor transmission measurements

The films were equilibrated at 50 ± 2% RH and 22 ± 1 °C (climate room) for 30 h minimum before performing the water vapor transmission measurements. After the equilibration, the films were mounted in Payne cups (TQC Sheen) with a circular 10 cm^2 open area. In some cases, the exposed area of the films was reduced with aluminum masks (hole area: 5 cm^2, MOCON Inc.). For the 0–50% RH measurement, 5 g of dry calcium chloride powder was placed inside the cup before mounting the film. Then the total weight was measured as a function of time, which was used to calculate the water vapor transmission rate (WVTR) and permeability (WVP). The increase in the weight of the cups, due to moisture absorption by the desiccant from the atmosphere, was noted to generate a plot of weight change versus time and a slope "*n*". The WVTR and WVP were calculated using the following equations:

$$WVTR = \frac{n}{A} \tag{2}$$

$$WVP = \frac{WVTR \cdot l}{\Delta p} \tag{3}$$

where A, l, and Δp are the area, thickness, and water vapor pressure difference over the film. After the 0–50% RH measurement, the film was carefully removed and kept separately and safely in the humidity room for equilibration at 50% RH for a minimum of 30 h. The $CaCl_2$ was removed from the cup and the cup was cleaned and kept in the same room in a dust-free place. Meanwhile, the cup was filled with 2 or 5 mL of water, which corresponds to a level of ≈1/4th of the height of the cup. After the equilibration, the films were again mounted in the cup and the mass change (due to the outflow of water from the 100% RH condition to the surrounding 50% RH environment) was recorded as a function of time. The mass change was used to calculate the water vapor transmission rate and permeability. To account for that the water vapor pressure at the film surface differs from that (100% RH) over the water (due to the air gap inside the cup), the corrected WVTR (and WVP) was calculated as described in Gooding et al.[33] All measurements were performed in at least duplicates and their average values were reported.

3. Results and Discussion

Two CNC/glucose (GLU) films with different structural colors were investigated in the present study: a green-colored (CNC/GLU = 52/48) and a red-colored (CNC/GLU = 39/61) film (Figure 2a,b). These were prepared via self-assembly under evaporation-driven conditions. Their UV–vis total transmittance spectra are included in Figure 2c. The spectrum for a pristine CNC film without GLU can be found in the Supporting Information (Figure S1, Supporting Information). The transmittance spectrum for the 84 ± 11 µm thick green film (CNC/GLU = 52/48) exhibited a broad dip in transmission at ≈510 nm. With increased glucose content (CNC/GLU = 39/61, film thickness 50 ± 3 µm), the pitch increased further, and a red shift in the transmission dip occurred, which is in concordance with previous studies on CNC/glucose films.[16] In Figure 2d,e, polarized optical microscopy (POM) images (linearly polarized light, reflectance mode) of the films are presented. Each film had a macroscopic dominating color (Figure 2), but for both films additional colors were present. The colored regions were separated by grain boundaries (Figure 2d,e). The presence of such different colors in a single film has been speculated to be due to spatial differences in the local helical axis orientation and/or deviations in the equilibrium pitch (Figure 2f).[21] Due to the hygroscopicity, the CNC-based films are prone to absorb moisture, which increases the pitch and causes a red shift as shown in Figure 2g. The moisture uptake is a function of the relative humidity and temperature, and for CNC films it is low below ≈60% RH (e.g., at 23 °C), but increases exponentially above this threshold.[22] Besides the change in pitch/color, we note that the moisture uptake at high relative humidity can rapidly trigger the crystallization of glucose (Figure 2h,i). The film in Figure 2h contained such glucose crystals, which were obtained after several months of storage (approximately June to February) at ambient indoor conditions. During that period the relative humidity reaches over 60% (July/August).[23] Hence, there is a need to protect films from high-moist environments. On the other hand, storage in dry conditions[24] or at ≈50% RH (7 weeks tested) and 21–22 °C did not alter the visual appearance of the films.

To solve the moisture problem, we here laminated structurally colored CNC/GLU photonic films between two thin synthetic cuticle films. A systematic study was recently performed using 16-hydroxyhexadecanoic acid (HHA) and glycerol for synthetic cuticle synthesis.[4] In the present study, we exploited the findings in that study and specifically worked with the polyester film with an HHA: glycerol molar ratio of 3:1 for the synthetic cuticle membrane (here referred to as HG31), see **Figure 3**. This is due to the best combination of mechanical flexibility and moisture barrier properties of the film attained at that composition.[4] Thick synthetic cuticle films were prepared using a specific compression molding protocol (Experimental section). These were then made thinner using an

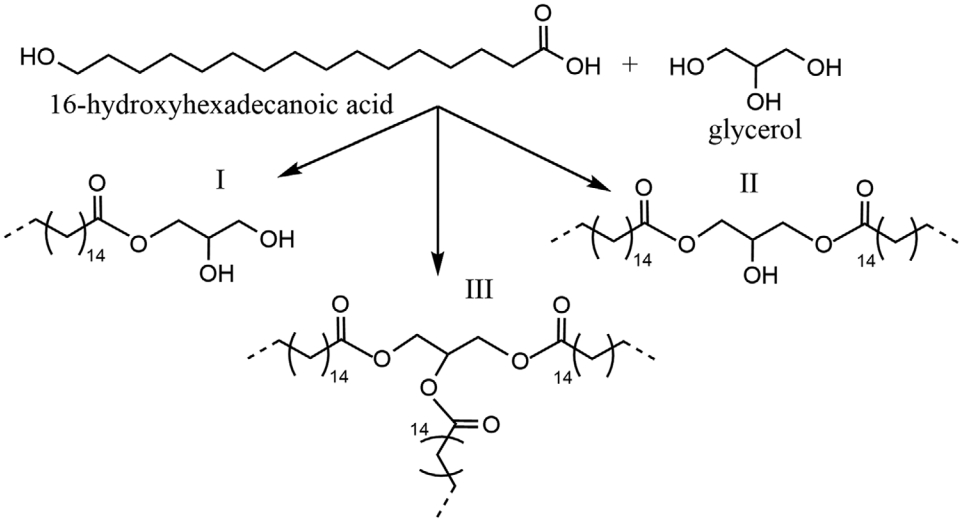

Figure 3. Synthesis of the HHA: glycerol polyester. Three possible reaction products are included. A fourth reaction includes one primary and one secondary glycerol alcohol reacting with HHA.

ADVANCED MATERIALS INTERFACES
Open Access
www.advmatinterfaces.de

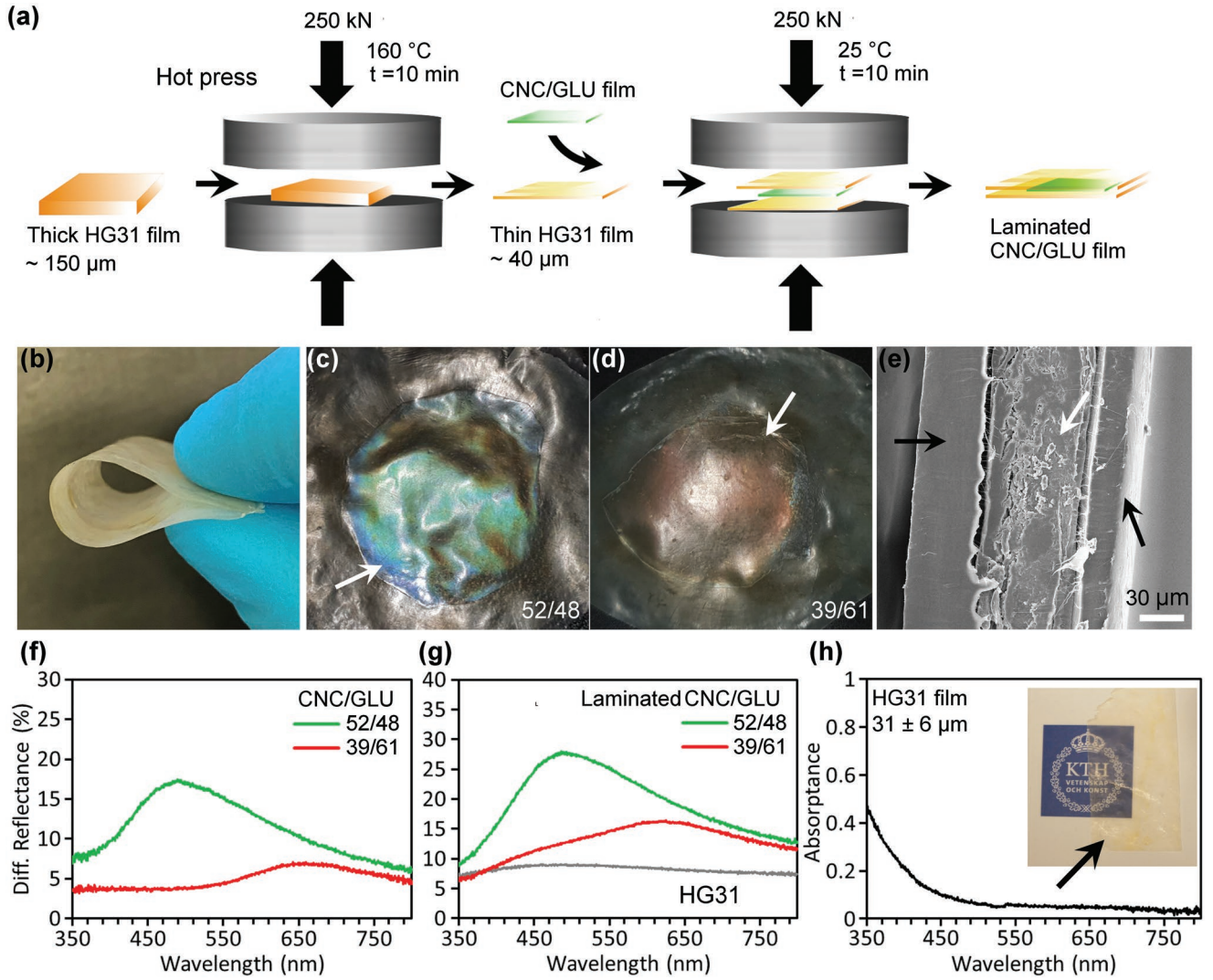

Figure 4. a) Illustration of the lamination process where the CNC/GLU film is sandwiched between thin HG31 films. b) Photograph of a thin HG31 film. c,d) Photographs of the HG31-laminated CNC/GLU films and e) SEM image of a cross-section of a laminated CNC/GLU film (CNC/GLU: 52/48). The white arrow points to the CNC/GLU film and the black arrows point at the HG31 layers. Diffuse reflectance spectra (integrating sphere) of f) CNC/GLU films and g) CNC/GLU films laminated with HG31 films and a neat HG31 film. h) Absorptance of an HG31 film. Inset: an HG31 film, black arrow. Measurements (f–h) performed at 21 ± 2% RH and 21 °C.

additional hot-pressing step (250 kN, 160 °C, 10 min) and two of the thin HG31 films were used to cover each side of the CNC/GLU film and compressed (see the schematic of the production protocol in **Figure 4**a). The average thicknesses of the synthetic cuticle films were in the range of ≈30–40 µm, which rendered the coatings transparent (Figure S2, Supporting Information). In Figure 4b, a photograph of a thin HG31film is included demonstrating the flexibility of this film and the resulting polyester-coated CNC/GLU sandwich films are presented in Figure 4c,d. A sandwich cross-section observed with SEM (Figure 4e), disclosed the lamellar structure, with the CNC/GLU film surrounded by HG31 films. Visual comparison of pristine CNC/GLU (52/48 and 39/61) photonic films (Figure 2a,b) and their subsequent coated sandwich structures (Figure 4c,d), revealed that on the macroscopic scale, the predominant color (green and red) was approximately the same before and after coating. This was further confirmed when studying the diffuse reflectance of the CNC/GLU films and the HG31-laminated CNC/GLU films (Figure 4f,g). The thickness of the CNC/GLU films was 75 ± 17 µm (52/48) and 43 ± 11 µm (39/61), whereas the thickness of the HG31-laminated CNC/GLU films was 167 ± 19 µm (laminated, CNC/GLU = 52/48) and 127 ± 15 µm (laminated, CNC/GLU = 39/61). The thickness of the HG31 coatings (on each side) in these sandwich structures were 37 ± 8 µm (52/48) and 39 ± 10 µm (39/61), measured with a Mitutoyo thickness meter. Because the synthetic cuticle layers were thin, the absorptance and total transmittance of the coating was low and high, respectively, at wavelengths above ≈440 nm (Figure 4h; Figure S2, Supporting Information). The rough surface of the synthetic cuticle membrane, as a consequence of the pressing procedure, is shown in Figure S3 (Supporting Information).

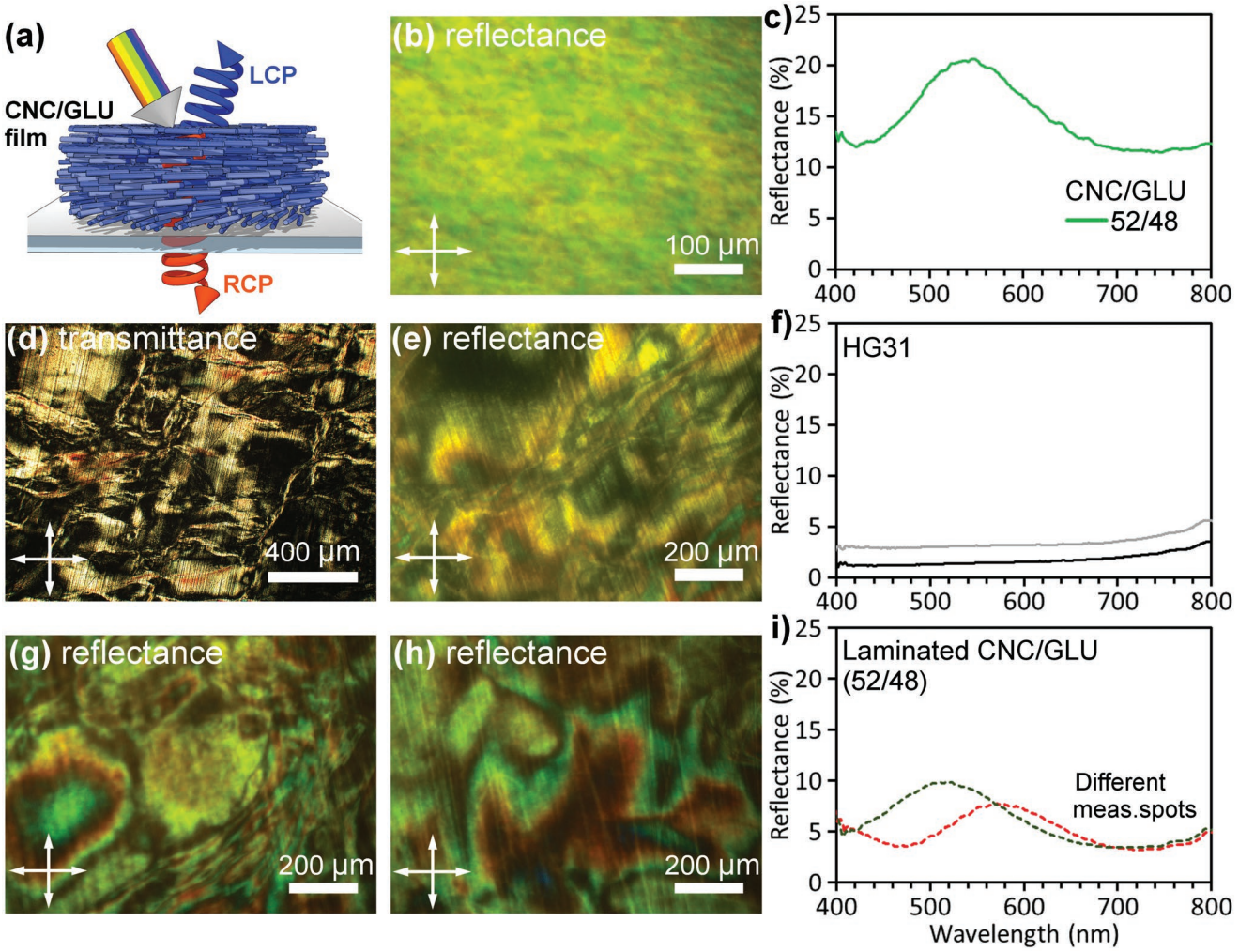

Figure 5. a) Schematic of reflected and transmitted circularly polarized light through a CNC/GLU film. POM image in reflectance mode (linearly polarized light) of b) a CNC/GLU (52/48) film, and c) reflectance spectrum (using linearly polarized incident light only) of the (52/48) CNC/GLU film. POM images of the synthetic cuticle (HG31) in d) transmission mode and e) reflectance mode and f) reflectance spectra (only incident linearly polarized light) obtained at two different spots on the HG31 film. In g,h) POM images of the synthetic cuticle-laminated CNC/GLU (52/48) film at two different locations. In i) reflectance spectra (only linearly polarized incident light) taken at two different locations on the synthetic cuticle-laminated CNC/GLU (52/48) film. Reflectance spectra (c,f,i) were obtained with identical image acquisition settings. All the POM images taken with crossed polarizers (denoted by crossed arrows).

To further characterize the structural colors of the sandwich on the microscopic scale, POM studies were performed, with the results shown in **Figure 5** and in Figures S4–S8. The POM image, taken in reflectance mode between crossed linear polarizers, of the neat green CNC/GLU film is presented in Figure 5b. The reflectance spectrum was obtained using linearly polarized incident light only, Figure 5c (the analysis of the red CNC/GLU film is found in Figure S4, Supporting Information). In accordance with the results in Figure 2, the reflectance peak (Figure 5c) was quite broad, with non-negligible reflection in the blue, green, and red spectral ranges. It is well known that structurally colored CNC/GLU films preferentially interact with the component of light that is left-handed circularly polarized (LCP), such that the reflected light (Figure 5b,c, predominantly green, but also blue and red colors) from a CNC/GLU film will be LCP, as schematically depicted in Figure 5a. Right-handed circularly polarized (RCP) light, on the other hand, will be transmitted through the CNC/GLU film. In other words, if the incident light is RCP light then the film will appear dark in reflection.[7,16,25]

POM images in transmission and reflection mode (linearly polarized light, crossed polarizers) for the neat synthetic cuticle film are shown in Figure 5d,e, respectively. Some colors, mostly green and red due to interference, were observed. The synthetic cuticle polymer used herein is semi-crystalline and cross-linked/branched (Figure 3), as reported previously,[4] and hence we hypothesize that this, in combination with the extension/orientation of the film experienced during hot-pressing, resulted in local birefringent properties of the membranes. The local birefringence was further confirmed by rotating a neat synthetic cuticle film between crossed polarizers in transmission mode (Figure S5, Supporting Information). From those results, it is clearer that the HG31 polymer chains were locally organized in varyingly sized regions, and with the direction

of the ordinary and extraordinary refractive indices in these regions alternating over the surface of the HG31 film. Other areas remained completely dark during rotation, suggesting the absence of birefringent properties in those areas. Reflectance results, using only linearly polarized incident light, obtained from microscopic areas that appeared red or green during imaging confirm that those areas did not correlate with any red or green reflectance peaks for the neat HG31 film (Figure 5f and measurement spots given in Figure S6 (Supporting Information), using the same acquisition settings as for the CNC/GLU films [Figure 5c]). The same trend was seen all across the synthetic cuticle film and the reflectance from these microscopic areas was instead comparable to the diffuse reflectance measured for macroscopic areas of the synthetic cuticle film (Figure 4g).

In the case of the synthetic cuticle laminated green CNC/GLU film (the HG31-laminated red CNC/GLU film is presented in Figure S7, Supporting Information), the reflected portion of the light depends both on the optical properties of (local birefringence) the synthetic cuticle film and the polarization-dependent reflectance of the underlying CNC/GLU film. Figure 5g,h displays the POM results for the CNC/GLU green film laminated with the synthetic cuticle. Colored regions of red, green, orange, and black were observed. When comparing Figure 5g,h with those of the bare CNC/GLU film (Figure 5b) and the synthetic cuticle (Figure 5e), it is clear that the synthetic cuticle coating influenced the optical response in certain areas. The reason is that any local birefringent properties of the cuticle film modify the polarization state of the incident linearly polarized light before it interacts with the underlying CNC/GLU film. The wavelengths reflected by the underlying CNC/GLU film were therefore contingent on any alteration of the incident light by the cuticle film, which depends on the wavelength of the incident light, the local birefringence and thickness of the synthetic cuticle, as previously exemplified when combining a birefringent liquid crystal layer with structurally colored CNC films.[7,16,25] However, we note that as the birefringent properties were not well-defined here and varied (or were absent) for different areas of the synthetic cuticle (Figure S5, Supporting Information), the reflected colors are also expected to vary over the surface of the cuticle laminated CNC/GLU film. Figure 5i presents the reflectance at two different measurement spots on the laminated CNC/GLU film, attained using linearly polarized incident light only (measurement spots indicated in Figure S8, Supporting Information). The perceived reflected colors were different at these two measurement spots, which could be due to variations in the original color of the CNC/GLU films and/or spatial variations in the birefringence of the cuticle layer. The latter can result in peak narrowing, compare the peaks in Figure 5i to that of the bare CNC/GLU film in Figure 5c. Peak narrowing would be due to the collective optical properties of a birefringent cuticle layer and the CNC/GLU film. In brief, the linearly polarized incident light can be decomposed into equal fractions of LCP and RCP light. The birefringent cuticle layer then enhances or suppress the fraction of LCP light reaching the CNC in a wavelength-dependent manner, which modifies the original reflectance peak of the CNC/GLU film. Similar complex optical responses on the microscopic scale, including peak narrowing, have previously been reported and discussed, for example when a chiral nematic CNC film is combined with an optically birefringent liquid crystal layer.[7,16]

The natural plant cuticle protects against moisture loss and to test whether the moisture barrier properties in our synthetic cuticle film would exhibit a similar function for the CNC/GLU material, the moisture permeation was measured. However, here protection is most important at high relative humidity. This is because the moisture uptake by the CNC/GLU films at low RH (0–50%) is minute, resulting in a water vapor permeability (WVP) of the bare CNC/GLU films that is comparable to that of the HG31. The measured water vapor permeability coefficient, WVP, (obtained at 0–50% RH gradient) for the green CNC/GLU film was 11.3 (±1.2) × 10^4 g μm m^{-2} day^{-1} atm^{-1} and for the red CNC/GLU film it was 12.5 (±5.6) × 10^4 g μm m^{-2} day^{-1} atm^{-1}, which can be compared to that of the HG31 (8.0 (±0.7) × 10^4 g μm m^{-2} day^{-1} atm^{-1}). At low relative humidity, a protective synthetic cuticle membrane is not necessarily needed, in particular as glucose crystallization was also not observed at ≈50% RH, 21–22 °C (tested storage time of 7 weeks). The excellent barrier properties of CNC/GLU films themselves at lower RH are due to that few water molecules are sorbed in the interior of the film[22] and, hence, water contributes very little to increasing permeation (it does not swell/plasticize the system). Factors that add to the good barrier properties at low RH are the impermeable crystalline domains of CNCs, the chiral CNC nematic packing and the extensive hydrogen bond network.[26] The reduction in permeability, with the synthetic coating present, is expected to be more pronounced at higher RH, and to test this we looked closer at the cuticle-laminated CNC film with the highest glucose content. **Table 1** presents results for the synthetic cuticle laminated CNC/GLU (39/61) film, the bare CNC/GLU (39/61) film, and the bare synthetic cuticle coating at high relative humidity conditions (50–100% RH gradient).

Water is an effective plasticizer. Hence, at higher RH the important polymer-to-polymer hydrogen bonds (CNC-CNC, CNC-glucose) are reduced in density, leading to high water permeation.[22,27] This occurred for the hygroscopic CNC/GLU film, resulting in more than two orders of magnitude increase in WVP (Table 1).

On the contrary, the WVP only increased slightly for the synthetic cuticle film, on average from 8.0 × 10^4 to 8.6 × 10^4 g μm m^{-2} day^{-1} atm^{-1}. The same trend, with only a small, if any, increase in WVP with increasing RH, has been observed for other relatively hydrophobic polymers, such as PLA.[28,30] The moisture permeability of HG31 can be further compared to those of common polymers, see Table 1. The HG31 film had a value that was significantly lower than that of the hydrophilic PVOH, but similar to the semi-hydrophobic aromatic polyester (PET), hydrophobic PS, and semi-hydrophobic PVC. However, the moisture permeability is higher than for a fully hydrophobic PP and high-crystalline PVDC. It should be noted that the reported data in Table 1 for the common polymers correspond to a condition of 85% relative humidity. However, all the materials, except PVOH, are considered not to depend significantly on the actual relative humidity.

Introducing a moisture-protective synthetic cuticle layer on top of the CNC/GLU film led to a significant decrease in WVP (and WVTR). In fact, the WVP decreased by more than two

Table 1. WVTR and WVP for the CNC/GLU film, the synthetic cuticle (HG31), and the synthetic cuticle laminated CNC/GLU film, in a 50–100% RH gradient. Values of common polymers are also given as a comparison.

Sample	WVTR [g m^{-2} day^{-1}]	WVP [g µm m^{-2} day^{-1} atm^{-1}]
CNC/GLU (39/61)	6500 ± 400	$2.1 \times 10^7 \pm 1.3 \times 10^6$
Synthetic cuticle (HG31)	20 ± 0.2	$8.6 \times 10^4 \pm 0.6 \times 10^4$
Laminated CNC/GLU (39/61)	14 ± 2.3	$12.3 \times 10^4 \pm 1.9 \times 10^4$
Calculated value, Laminated CNC/GLU[a)]	–	$13.7 \times 10^4 \pm 0.7 \times 10^4$
Common Polymers		
Polylactic acid (PLA)[28]	–	$\approx 2.9 \times 10^5$
Poly(ethylene terephthalate) (PET)[29],b)]	–	$(2.1–8.3) \times 10^4$
Polypropylene (PP)[29],b)]	–	$(0.8–1.7) \times 10^4$
Polystyrene (PS)[29],b)]	–	$(4.2–16.6) \times 10^4$
Poly(vinyl chloride) (PVC)[29],b)]	–	$(4.2–8.3) \times 10^4$
Polyvinyl alcohol (PVOH)[29],b)]	–	12.6×10^5
Poly(vinylidene chloride) (PVDC)[29],b)]	–	0.4×10^4

a)Calculated value for the synthetical cuticle laminated CNC/GLU (39/61); b)Testing conditions: 23 °C and 85% RH.

orders of magnitude (at high RH) (Table 1). Indeed, the sandwich had a quite low WVP, on the same order of magnitude as PS. The measured WVP for the synthetic cuticle laminated CNC/GLU film (12.3×10^4 g µm m^{-2} day^{-1} atm^{-1}), matched well with the calculated WVP, $13.7 \times 10^4 \pm 0.7 \times 10^4$ g µm m^{-2} day^{-1} atm^{-1} (Table 1), derived from the laminate equation:[31]

$$\frac{t_{tot}}{P_{tot}} = \frac{t_{HG31}}{P_{HG31}} + \frac{t_{CNC/GLU}}{P_{CNC/GLU}} \quad (4)$$

where t_{tot}, $t_{HG31,}$ and $t_{CNC/GLU}$ are the thicknesses for the synthetic cuticle laminated CNC/GLU film, the HG31 laminate film, and the protected CNC/GLU film, respectively. P_{HG31} and $P_{CNC/GLU}$ are the permeability coefficients of the two individual components. An important consequence, of a fixed relative humidity gradient over the laminated CNC/GLU film (such as a 50–100% RH gradient), is that the protective HG31 layer will lower the surface moisture concentration in the CNC/GLU films at the higher %RH side to a value lower than that of an unprotected CNC/GLU film. This is because the partial moisture pressure on the 100% RH side of the synthetic cuticle ($p_{100\%RH}$) will decrease over the thickness of the synthetic cuticle to a lower partial pressure value on the CNC/GLU side (p_2, i.e., $p_2 < p_{100\%RH}$). This drop is due to the low WVP of the synthetic cuticle coating and also depends on the coating thickness. The solubility (S) times the partial moisture pressure (p) gives the moisture content within the material, that is $C = Sp$, where C is the moisture concentration in the material. Hence, the surface moisture concentration will be lower in the protected CNC/GLU film ($p_2 < p_{100\%RH} = Sp_2 < Sp_{100\%RH} = C_2 < C_{100\%RH}$). Decreasing the moisture content in the CNC/GLU film is important as glucose crystallization should be minimized.

The staggering drop in WVP is attributed to the crystallinity and the high hydrophobicity of the protective HG31 film, similar to that observed in the natural plant cuticles. The HG31 chemical structure (similar to PE, except for the sparsely occurring ester groups) and the film surface roughness (which may delay further diffusion into the polymer), mainly contribute to the hydrophobic character that can be advantageously used to reduce and delay moisture uptake and glucose crystallization in the vulnerable CNC/GLU films.[6]

4. Conclusion

In summary, we presented a biomimetic strategy for reducing the rate of moisture uptake in structurally colored CNC/GLU films. The synthetic cuticle coating resembled nature's own protective coating, being a branched/crosslinked polyester (cutin) with a rough surface, mimicking the rough wax layer in plants. The lamination made the CNC film stable in highly moist conditions; it reduced the water permeance through the film by more than two orders of magnitude. This is the first demonstration of how to combine a moisture-protective and partially birefringent synthetic cuticle with a nanophotonic CNC-based material, where the dominant structural color of the nanophotonic CNC-based material is still present after coating. While highly transparent at the present thickness (≈30 µm), we also showed that the synthetic cuticle layer provided local birefringent properties that likely modified the optical response of the polarization-dependent structural colors at those sites. Further control of the production, focusing on the cuticles' birefringent properties, would enable more complex nanophotonic materials, that augment certain colors upon light changes.

Supporting Information

Supporting Information is available from the Wiley Online Library or from the author.

Acknowledgements

P.R.A., S.S., and D.B. contributed equally to this work. P.R.A., A.J.S., and M.J. acknowledge the funding from the Olle Byggmästare (Grant No. 194–0679). M.H., and S.S. acknowledge support from the Knut and Alice Wallenberg Foundation (WWSC), M. J. and D.B. acknowledge support from Linköping University and industry through the Wallenberg Wood Science Center; the Swedish Government Strategic Research Area in Materials Science on Functional Materials at Linköping University (Faculty Grant SFO-Mat-LiU No. 2009 00971).

Conflict of Interest

The authors declare no conflict of interest.

Data Availability Statement

The data that support the findings of this study are available from the corresponding author upon reasonable request.

Keywords

cellulose nanocrystals, moisture barrier, structural colors, synthetic plant cuticle

Received: October 25, 2022
Published online: January 20, 2023

[1] a) K. Koch, B. Bhushan, W. Barthlott, *Soft Matter* **2008**, *4*, 1943; b) C. Buschhaus, R. Jetter, *J. Exp. Bot.* **2011**, *62*, 841; c) E. Domínguez, J. A. Heredia-Guerrero, A. Heredia, *New Phytol.* **2011**, *189*, 938; d) T. H. Yeats, J. K. Rose, *Plant Physiol.* **2013**, *163*, 5.
[2] M. Riederer, L. Schreiber, *J. Exp. Bot.* **2001**, *52*, 2023.
[3] a) B. B. Buchanan, W. Gruissem, R. L. Jones, *Biochemistry & Molecular Biology of Plants*, American Society of Plant Physiologists, Rockville, MD **2000**.
[4] S. Singha, V. Gowda, M. S. Hedenqvist, *ACS Appl. Polym. Mater.* **2021**, *3*, 4088.
[5] a) S. F. Osman, H. C. Gerard, W. F. Fett, R. A. Moreau, R. L. Dudley, *J. Agric. Food Chem.* **1995**, *43*, 2134; b) S. F. Osman, P. Irwin, W. F. Fett, J. V. O'Conno, N. Parris, *J. Agric. Food Chem.* **1999**, *47*, 799; c) J. A. Heredia-Guerrero, A. Heredia, E. Domínguez, R. Cingolani, I. S. Bayer, A. Athanassiou, J. J. Benítez, *J. Exp. Bot.* **2017**, *68*, 5401; d) J. A. Heredia-Guerrero, A. Heredia, R. García-Segura, J. J. Benítez, *Polymer* **2009**, *50*, 5633; e) J. J. Benítez, J. A. Heredia-Guerrero, S. Guzmán-Puyol, E. Domínguez, A. Heredia, *J. Appl. Polym. Sci.* **2015**, *132*, 41328; f) A. Manrich, F. K. Moreira, C. G. Otoni, M. V. Lorevice, M. A. Martins, L. H. Mattoso, *Carbohydr. Polym.* **2017**, *164*, 83; g) J. A. Heredia-Guerrero, J. J. Benítez, P. Cataldi, U. C. Paul, M. Contardi, R. Cingolani, I. S. Bayer, A. Heredia, A. Athanassiou, *Adv. Sustainable Syst.* **2017**, *1*, 1600024; h) W. Lu, J. E. Ness, W. Xie, X. Zhang, J. Minshull, R. A. Gross, *J. Am. Chem. Soc.* **2010**, *132*, 15451.
[6] J. A. Kelly, M. Giese, K. E. Shopsowitz, W. Y. Hamad, M. J. MacLachlan, *Acc. Chem. Res.* **2014**, *47*, 1088.
[7] S. N. Fernandes, P. L. Almeida, N. Monge, L. E. Aguirre, D. Reis, C. L. P. de Oliveira, A. M. F. Neto, P. Pieranski, M. H. Godinho, *Adv. Mater.* **2017**, *29*, 1603560.
[8] W. Song, J.-K. Lee, M. S. Gong, K. Heo, W.-J. Chung, B. Y. Lee, *ACS Appl. Mater. Interfaces* **2018**, *10*, 10353.
[9] T. Lu, H. Pan, J. Ma, Y. Li, S. W. Bokhari, X. Jiang, S. Zhu, D. Zhang, *ACS Appl. Mater. Interfaces* **2017**, *9*, 18231.
[10] K. Yao, Q. Meng, V. Bulone, Q. Zhou, *Adv. Mater.* **2017**, *29*, 1701323.
[11] a) L. Chen, C. Lai, R. Marchewka, R. M. Berry, K. C. Tam, *Nanoscale* **2016**, *8*, 13288; b) L. Chu, X. Zhang, W. Niu, S. Wu, W. Ma, B. Tang, S. Zhang, *J. Mater. Chem. C* **2019**, *7*, 7411; c) S.-Y. Liu, Y.-B. Gong, S. Ma, Y.-H. Wang, L. Gan, J. Huang, *Chin. J. Polym. Sci.* **2020**, *38*, 1061.
[12] M. Gu, C. Jiang, D. Liu, N. Prempeh, I. I. Smalyukh, *ACS Appl. Mater. Interfaces* **2016**, *8*, 32565.
[13] R. Shanker, P. R. Anusuyadevi, S. Gamage, T. Hallberg, H. Kariis, D. Banerjee, A. J. Svagan, M. P. Jonsson, *ACS Nano* **2022**, *16*, 10156.
[14] C. Sun, D. Zhu, H. Jia, C. Yang, Z. Zheng, X. Wang, *ACS Appl. Mater. Interfaces* **2020**, *12*, 26455.
[15] Q. Li, M. Guo, D. Liu, H. Qiao, W. Gustave, N. Prempeh, Y. Cai, J. Peng, *Ind. Eng. Chem. Res.* **2021**, *60*, 8776.
[16] P. R. Anusuyadevi, R. Shanker, Y. Cui, A. V. Riazanova, M. Jarn, M. P. Jonsson, A. J. Svagan, *Adv. Mater.* **2021**, *33*, 2101519.
[17] F. Su, D. Liu, M. Li, Q. Li, C. Liu, L. Liu, J. He, H. Qiao, *Carbohydr. Polym.* **2020**, *233*, 115843.
[18] M. Xu, W. Li, C. Ma, H. Yu, Y. Wu, Y. Wang, Z. Chen, J. Li, S. Liu, *J. Mater. Chem. C* **2018**, *6*, 5391.
[19] T. Wu, J. Li, J. Li, S. Ye, J. Wei, J. Guo, *J. Mater. Chem. C* **2016**, *4*, 9687.
[20] S. Thomas, S. Ravishankaran, N. A. J. A. Justin, A. Asokan, T. M. J. Kalsingh, M. T. Mathai, N. Valecha, J. Montgomery, M. B. Thomas, A. Eapen, *Malar. J.* **2018**, *17*, 201.
[21] R. M. Parker, G. Guidetti, C. A. Williams, T. Zhao, A. Narkevicius, S. Vignolini, B. Frka-Petesic, *Adv. Mater.* **2018**, *30*, 1704477.
[22] S. Shrestha, J. A. Diaz, S. Ghanbari, J. P. Youngblood, *Biomacromolecules* **2017**, *18*, 1482.
[23] (Eds.: J. Arfvidsson, L.-E. Harderup, I. Samuelson), *Fukthandbok : praktik och teori*, Svensk Byggtjänst, Stockholm **2017**.
[24] B. Makower, W. B. Dye, *J. Agric. Food Chem.* **1956**, *4*, 72.
[25] J. A. De La Cruz, Q. Liu, B. Senyuk, A. W. Frazier, K. Peddireddy, I. I. Smalyukh, *ACS Photonics* **2018**, *5*, 2468.
[26] D. Qu, H. Zheng, H. Jiang, Y. Xu, Z. Tang, *Adv. Opt. Mater.* **2019**, *7*, 1801395.
[27] J. Wang, D. J. Gardner, N. M. Stark, D. W. Bousfield, M. Tajvidi, Z. Cai, *ACS Sustainable Chem. Eng.* **2018**, *6*, 49.
[28] S. S. Karkhanis, N. M. Stark, R. C. Sabo, L. M. Matuana, *Composites, Part A* **2018**, *114*, 204.
[29] J. Lange, Y. Wyser, *Packag. Technol. Sci.* **2003**, *16*, 149.
[30] R. A. Auras, B. Harte, S. Selke, R. Hernandez, *J. Plast. Film Sheeting* **2003**, *19*, 123.
[31] J. Crank, E. P. J. Crank, *The Mathematics of Diffusion*, Clarendon Press, Oxford **1979**.
[32] J. J. Benítez, J. A. Heredia-Guerrero, M. A. Cruz-Carrillo, M. J. Barthel, H. E. Knicker, A. Heredia, *J. Appl. Polym. Sci.* **2017**, *134*, 44350.
[33] A. Gennadios, C. L. Weller, C. H. Gooding, *J. Food Eng.* **1994**, *21*, 395.